Physica Scripta. Vol. 32, 236–247, 1985

For Infra-Red Peaks in Molecular Liquids?

M. W. Evans

Department of Physics, U.C.N.W., Bangor, Gwynedd, Wales

S. I. Abas

Department of Applied Mathematics and Computation, U.C.N.W., Bangor, Gwynedd, Wales

G. J. Evans

Department of Chemistry, U.C.W., Aberystwyth, Dyfed, Wales

and

C. J. Reid

Mile-Stone Cottage, Pont Seni, Powys, Wales

Received May 29, 1984; accepted June 28, 1985

Abstract

Circular diffusion in a multiple cosine potential-energy well produces peaks in the far infra-red power absorption coefficient as the rate of escape from these wells becomes slow. The Kramers equation governing the dynamics of the system is solved using matrix inversion methods. The dependence of the number, relative intensity and frequency of the far infra-red peaks on matrix size is illustrated, and numerical results are shown describing the development with decreasing rate of escape of far infra-red peaks. The complete dielectric loss profile is shown to be a broad band of constant half-width 1.12 decades at low frequency, superimposed on which are the high frequency far infra-red peaks. The far infra-red power absorption spectrum in the deterministic limit of well-known models corresponding to the first three approximants of the linear Mori continued fraction expansion of the Liouville equation is shown to be composed of delta functions at well-defined frequencies. The number of delta functions increases with approximate order (i.e. number of continued fractions).

These theoretical results are discussed in terms of the recent experimental discovery by G. J. Evans of peaks in the far infra-red power absorption of dipolar and non-dipolar molecular liquids, and in terms of the recent suggestion by Grigolini and co-workers of a phase change in the low friction limit caused by deterministic transition to chaos.

Introduction

The first description of rotational diffusion was given, effectively, in terms of a rotational Langevin equation. In three dimensions this is a technically difficult problem [1], and for this reason a simple and clear solution is sought in terms of the equation:

$$I\ddot{\theta}(t) + I\beta\dot{\theta}(t) = \dot{w}(t) \tag{1}$$

where the rotation of the asymmetric top is confined to a plane. I is the effective moment of inertia associated with this motion, θ the angular displacement at the instant t, β the rotational friction coefficient and w a Wiener process. Eqn. (1) provides the autocorrelation functions:

$$\langle\dot{\theta}(t)\dot{\theta}(0)\rangle = e^{-\beta t}$$

$$\langle\cos\theta(t)\cos\theta(0)\rangle = \exp\left[-\frac{kT}{I\beta^2}\left[\beta t - 1 + e^{-\beta t}\right]\right]. \tag{2}$$

If it is assumed in eq. (1) that:

$$\beta \gg \frac{\ddot{\theta}(t)}{\theta(t)} \tag{3}$$

i.e. the "high friction" limit, then eqns. (2) produce:

$$\langle\cos\theta(t)\cos\theta(0)\rangle \doteq \exp\left[-\frac{kTt}{I\beta}\right]. \tag{4}$$

In this limit we can define the so-called Debye relaxation time as:

$$\tau_D = \frac{I\beta}{kT}. \tag{5}$$

Cumbersome solutions for the three dimensional diffusion of the asymmetric top from eqn. (1) have recently become available, but add little physical insight, if any.

This simple "one-particle" model has many short-comings, which have been documented. The need to account for "liquid structure" is probably the most obvious of these, and in this context the following modification has been proposed:

$$I\ddot{\theta}(t) + I\beta\dot{\theta}(t) + V'(\theta) = \dot{w}(t) \tag{6}$$

$$V = -V_0\cos(m\theta(t)) \tag{7}$$

and solved by Reid [2] by transforming into the Kramers equation:

$$\frac{\partial\rho}{\partial t} + \dot{\theta}\frac{\partial\rho}{\partial\theta} - \frac{V'}{I}\frac{\partial\rho}{\partial\theta} = \beta\frac{\partial}{\partial\dot{\theta}}\left[\dot{\theta}\rho + \frac{kT}{I}\frac{\partial\rho}{\partial\theta}\right] \tag{8}$$

for the conditional probability density function

$$\rho(\dot{\theta}, \theta, t|\dot{\theta}(0), \theta(0), 0).$$

The solution by Reid is much more transparent than others in the literature and opens up several new possibilities in the field of Langevin dynamics. This paper explores the case $\beta \to 0$, the opposite to the "high friction" limit mentioned already. In the limit $\beta \to 0$ it has been shown recently [3] that the rate of escape from the potential wells defined by eqn. (7) becomes very low, *and that this rate of escape becomes proportional to β itself*. When $\beta = 0$ eqn. (6) reduces to the deterministic result:

$$I\ddot{\theta}(t) + V'(\theta) = 0. \tag{9}$$

Furthermore, if the temperature is very low, the motion is confined to the bottom of the potential well, and:

$$\sin m\theta \doteq m\theta, \tag{10}$$

so that eqn. (9) gives the familiar Hooke's law:

$$I\ddot{\theta}(t) + V_0 m^2 \theta = 0. \tag{11}$$

In this respect eqn. (6) is *profoundly* different from eqn. (1), although superficially similar in appearance. There is no way of obtaining Hooke's law from eqn. (1). The link between the modified Langevin equation (6) and Hooke's law [eqn. (11)] is an important one, for it provides a route from liquid state molecular dynamics to the dynamics of molecular crystals. It is well-known [4] that the harmonic approximation [eqn. (11)] forms the basis for the available descriptions of the far infra-red lattice modes of crystalline solids. Eqn. (11) would describe the elementary oscillatory motion giving rise to *one* rotational lattice mode – a *delta function* of frequency. In contrast, Reid [2] has shown clearly that eqn. (6) produces for the far infra-red power absorption coefficient a *broad band* for the *relatively high* values of β given in his paper [see Fig. (3)].

It follows naturally from these considerations that the transition from eqn. (6) to eqn. (11) *describes the phase transition* from molecular liquid to molecular crystal. This apparently obvious and superficial remark has *profound* implications for the theory of Langevin dynamics, because such a phase change *must* be generated by the simple process:

$$\beta \to 0. \tag{12}$$

This means that solutions of eqn. (6) for molecular dynamics *must* produce lattice modes in the 'low-friction' limit. It follows that *there is no fundamental difference* between liquid and crystal dynamics in the framework of the modified Langevin equations and the equivalent Kramers equation (8).

This paper solves eqn. (8) in the limit $\beta \to 0$ for various types of potential V, and for the parameters defined by Reid [2]:

$$\alpha = \left(\frac{kT}{I}\right)^{1/2} \tag{13}$$

$$\gamma = \frac{V_0}{2(IkT)^{1/2}}. \tag{14}$$

The product $\alpha\gamma = V_0/2I$ is therefore a measure of the well depth in terms of the molecular moment of inertia I. In this paper $\alpha\gamma \gg \beta$ so that the rate of escape is low from relatively deep potential wells.

Numerical Solution of Eqn. (8)

Eqn. (8) can be written as:

$$mA(s) = A(0). \tag{15}$$

The square matrix m is an asymmetric complex, banded tri-diagonal, which must be inverted for the column vector $A(s)$, where s is the Laplace variable. The column vector $A(0)$ is the vector of initial values, arranged in the order:

$$\ldots A^0_{-r}(0), A^0_{-r+1}(0), \ldots, A^0_0(0), \ldots, A^0_{r-1}(0), A^0_r(0), \ldots;$$

$$\ldots A^1_{-r}(0), A^1_{-r+1}(0), \ldots, A^1_0(0), \ldots, A^0_{r-1}(0), A^1_r(0), \ldots;$$

and so on from top to bottom of the column $A(0)$.

The structure of the matrix m is given in Table 1, for a potential of the type:

$$V = -V_0 \cos(2\theta(t)). \tag{16}$$

The matrix m has the interesting and useful property illustrated in Table 2 for a potential of the more general type:

$$V = -V_0(\cos\theta(t) + \cos 2\theta(t) + \cos 3\theta(t) + \cos 4\theta(t) + \ldots). \tag{17}$$

Table 2 shows that adding terms to eqn. (16) has the effect of broadening a one diagonal band of the tri-diagonal matrix m. The overall structure of eqn. (15) therefore remains unchanged for the most general type of potential V, which can always by synthesised from a Fourier series expansion such as eqn. (17) provided this converges. Substituting eqn. (17) in eqn. (9) produces the result:

$$I\ddot{\theta}(t) + V_0(\sin\theta(t) + 2\sin 2\theta(t) + 3\sin 3\theta(t) + \ldots + M\sin M\theta(t) + \ldots) = 0 \tag{18}$$

Eqn. (18) is a non-linear, deterministic differential equation in θ, describing the elementary (one-molecule) oscillations of crystal dynamics. It is clear from inspection of eqn. (18) that *there are as many delta functions in the far infra-red spectrum from eqn. (18) as there are terms in the Fourier series, plus* cross terms, difference frequencies, overtones and so on. Looked upon in another way, m eigen frequencies in the far infra-red are generated by inverting the matrix m illustrated in Table 2 in the limit $\beta \to 0$.

The far infra-red power absorption coefficient is given [2] by:

$$\alpha(\omega) \propto \omega^2 [A^0_1(t) + A^0_{-1}(t)] \tag{19}$$

subject to the thermodynamic equilibrium initial conditions:

$$\langle \cos\theta(0) A^0_r(0) \rangle = \frac{1}{2\pi}\int_{-\pi}^{\pi} \cos\theta(0)\cos r\theta(0) \times \exp\left[2\left(\frac{\gamma}{\alpha}\right)\sum_M \cos M\theta(0)\right] d\theta(0)$$

$$-\frac{i}{2\pi}\int_{-\pi}^{\pi} \sin\theta(0)\cos r\theta(0) \times \exp\left[2\left(\frac{\gamma}{\alpha}\right)\sum_M \cos M\theta(0)\right] d\theta(0) \tag{20}$$

In this paper eqn. (15) is solved using the algorithm written by Reid [2], and also with a new algorithm written by M. W. Evans to incorporate potentials of the general type exemplified by eqn. (17). The latter algorithm inverts m by Crout factorization and partial pivotting, with extended precision arithmetic for the inner products on the CDC 7600 and CDC Cyber 205 computers of U.M.R.C.C., using the Numerical Algorithm Group's routine F04ADF. This algorithm was implemented in an efficiently vectorized form on the Cyber 205 with Pacific

Table I.

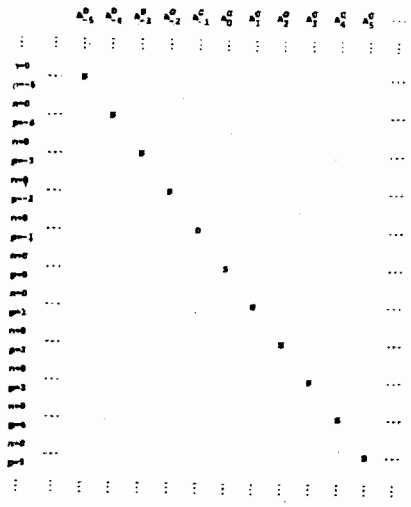

A

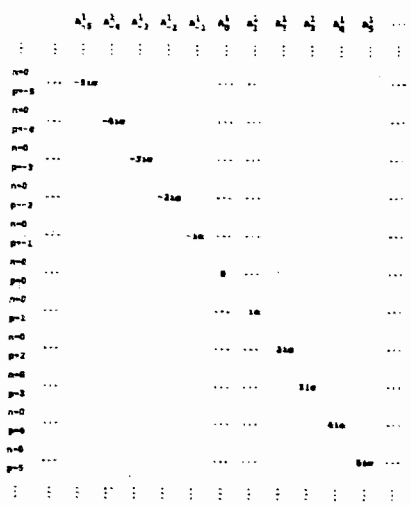

B

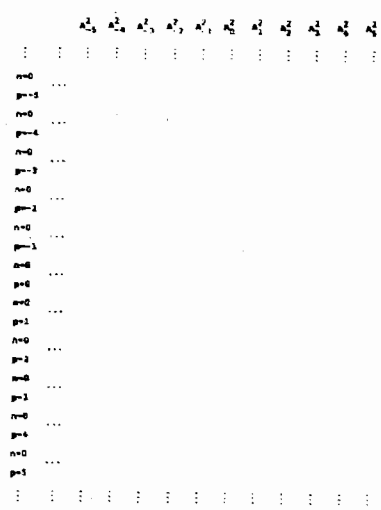

C

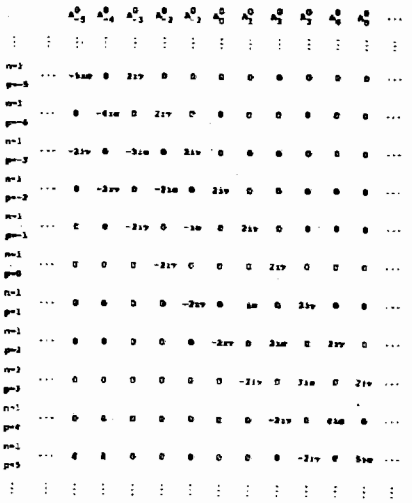

D_1

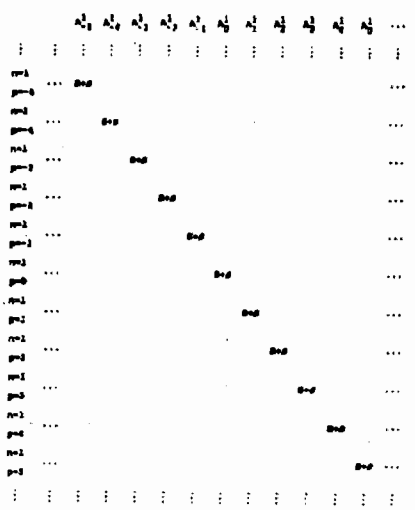

E

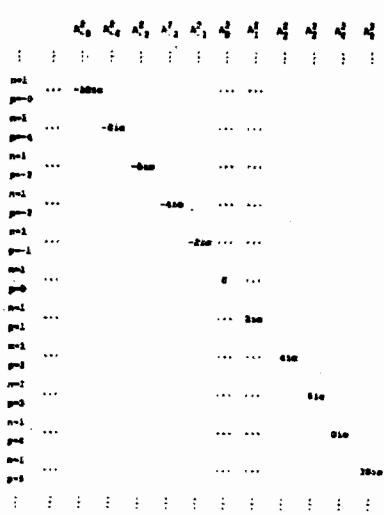

F

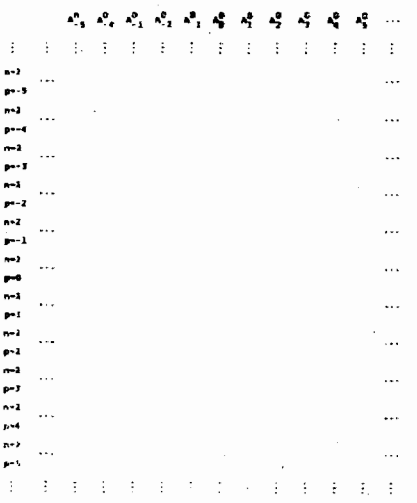

G

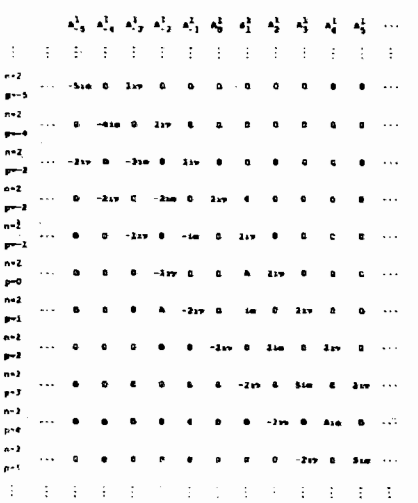

H_1

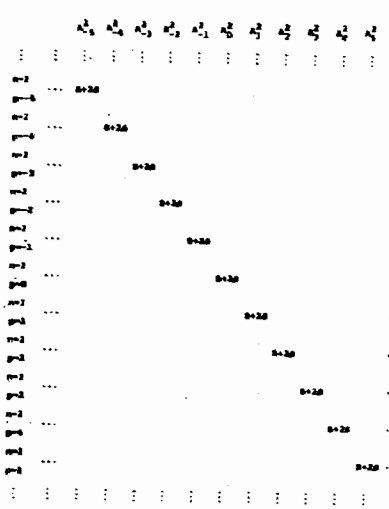

I

Table II.

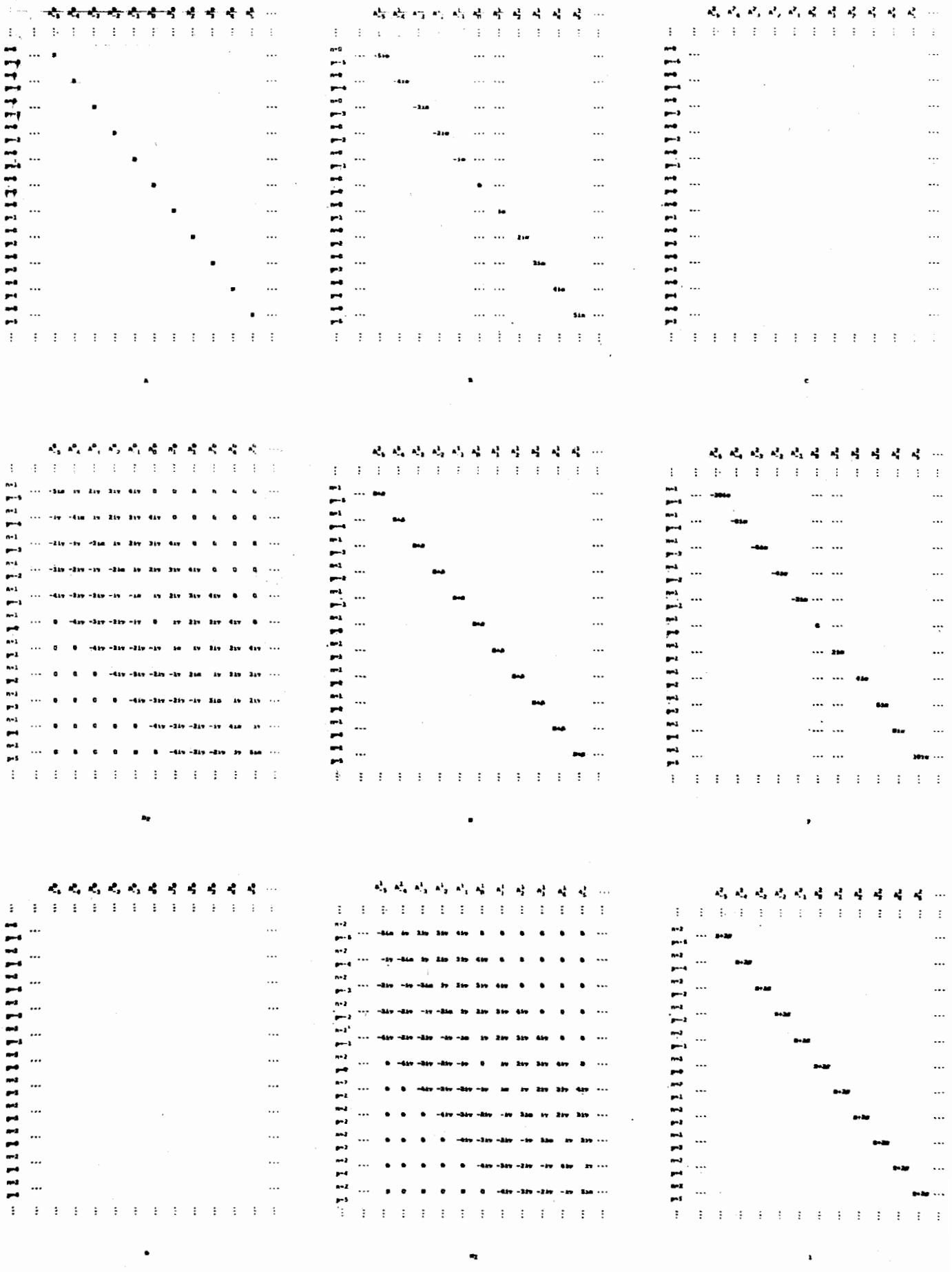

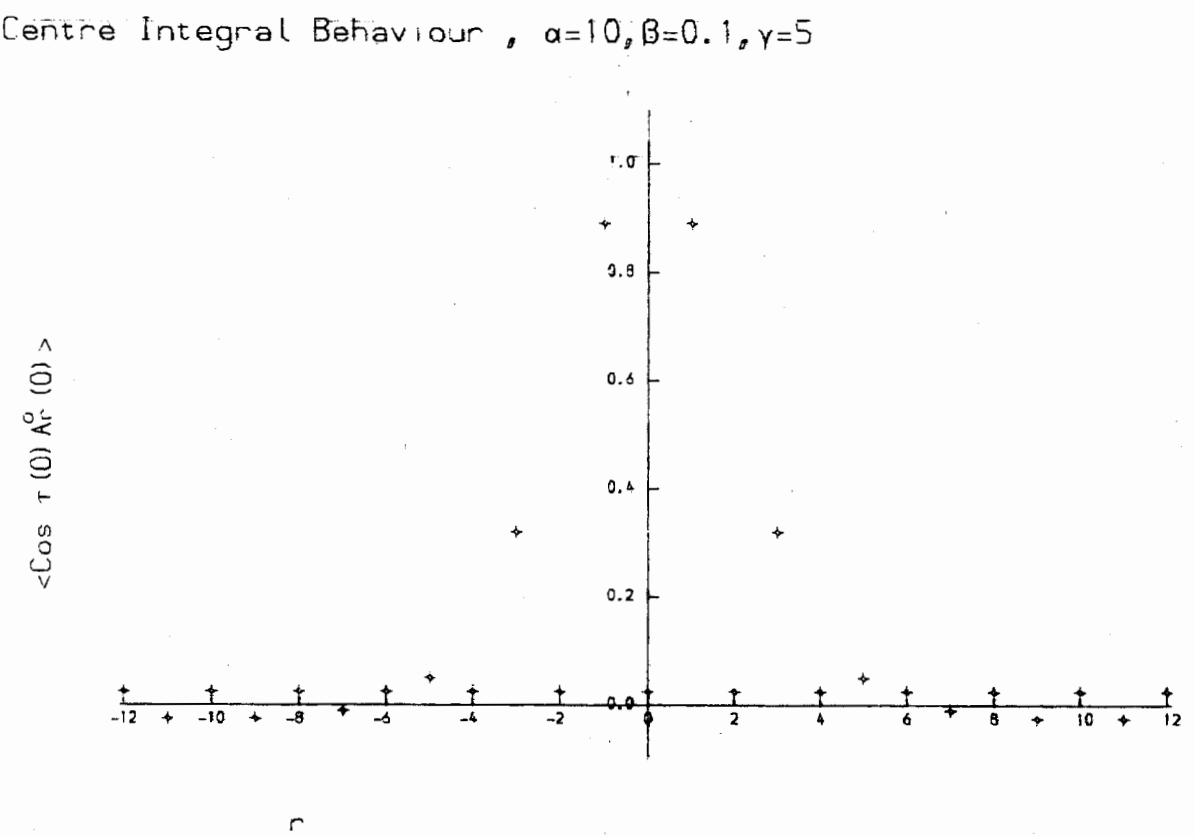

Fig. 1. Centre integral behaviour for $-12 \leq r \leq 12$. Ordinate: $\langle \cos\theta(0) A_r^0(0) \rangle$. Abscissa: r. The parameters are $\alpha = 10.0\,\text{THz}$; $\beta = 0.1\,\text{THz}$; $\gamma = 5.0\,\text{THz}$.

Sierra Research Incorporated's V.A.S.T. utility. This enabled the inversion of a 1000 x 1000 complex matrix $\boldsymbol{m}$ in under 200 secs C.P.U. Cyber time. The integrals in eqn. (20) were evaluated using the N.A.G. routine D01GAF. The precision of these integrations was checked by this routine for every integral, and also by using the fact that the complex part of eqn. (20) should vanish by symmetry. In respect of initial conditions it is important to note the relation:

$$\langle \cos\theta(0) A_r^m(0) \rangle = 0; \quad m \neq 0, \tag{21}$$

so that only the fifty or so centre integrals of the type (20) need to be evaluated in the column vector $\boldsymbol{A}(0)$.

Convergence effects and numerical artifacts

It is clear from inspection of eqns. (11) or (17) that in the limit $\beta \to 0$ peaks will appear in the far infra-red power absorption from modified Langevin equations and their equivalent Kramers equations. However, great care must be taken in calculating $\alpha(\omega)$ of eqn. (19) by inversion of $\boldsymbol{m}$, especially in the limit $\beta \to 0$. Reid has discussed [2] the convergence of eqn. (15) for relatively high values of β, where the far infra-red spectra is a broad band. In this section the behaviour of the Crout factorisation algorithm is reported for complex matrices $\boldsymbol{m}$ of the following dimensions:

(i) 100 x 100;
(ii) 200 x 200;
(iii) 400 x 400;
(iv) 1000 x 1000.

The dimensionality of matrix $\boldsymbol{m}$ (see Table 1) is defined by the product INCMAX (2NC + 1), where NC defines the number of centre integrals $A_{\pm r}^0(0)$ either side of $A_0^0(0)$. The behaviour of the $A_r^0(0)$ coefficients depends on the ratio γ/α. Convergence is much more rapid when this ratio is less than one. For $\alpha = 10.0\,\text{THz}$; $\gamma = 5.0\,\text{THz}$ the convergence behaviour as a function of r is illustrated in Fig. (1). Centre integral behaviour is independent of β, and, for $V = -V_0 \cos 2\theta(t)$, Fig. (1) shows that the terms $A_{\pm 1}^0(0)$, $A_{\pm 3}^0(0)$ and $A_{\pm 5}^0(0)$ dominate. The numerical integration produces within the uncertainty perfectly symmetrical results, i.e. $A_1^0(0) = A_{-1}^0(0)$; $A_3^0(0) = A_{-3}^0(0)$; $A_5^0(0) = A_{-5}^0(0)$. (It is interesting to speculate in this context a one to one correspondence between the number of significant centre integrals and number of significant peaks in the final far infra-red spectrum.) At $r = 0$, the uncertainty in the numerical integration is 2.9×10^{-6}, and at $r = \pm 12$ it is 1.6×10^{-4}. The value of the second integral in eqn. (20) is $< 10^{-3}$ for all $-12 \leq r \leq 12$, with an uncertainty for all r of $< 2 \times 10^{-6}$. These results were obtained with 100 quadrature input mesh points per integral. The value of π was used with machine precision with N.A.G. X01AAF.

The parameter INCMAX defines how many blocks of the type illustrated in Tables 1 and 2 are used to build up $\boldsymbol{m}$, which is always a square matrix.

The numerical method is based on the assumption [2] that the solution of eqn. (8) takes the general form:

$$\rho = \exp\left(-\frac{\dot{\theta}^2}{4\alpha^2}\right)\sum_n D_n\left(\frac{\dot{\theta}}{\alpha}\right)\phi_n(\theta, t) \qquad (22)$$

where D_n are modified Hermite polynomials – the Weber polynomials and $\phi_n(\theta, t)$ are expanded in a Fourier series:

$$\phi_n(\theta, t) = \sum_p A_p^n(t)\exp(ip\theta) \qquad (23)$$

($p = 0, \pm 1, \ldots, \pm\infty$). The parameter INCMAX therefore has the effect of truncating the series $\phi_n(\theta, t)$ of eqn. (23). It is also clear from the structure of Tables (1) and (2) that the values chosen for NC and INCMAX determine the level of truncation in eqn. (23).

The numerical results show that for any reasonable size of matrix m sensible results are obtained as $\beta \to 0$ from an expansion of the type (22) only if the ratio γ/α does not exceed approximately two. If this ratio becomes too high the far infra-red power absorption $\alpha(\omega)$ from eqn. (19) starts to show unphysical negative regions from *both* algorithms – the Reid method *and* Crout factorisation. This suggests that in this case the series (22) and (23) need many terms to converge, if they converge at all. This problem can be surmounted by using $\gamma/\alpha < 1$, even for very small m (of the order 100 x 100).

The question now arises of how the peaks in the far infra-red power absorption coefficient depend on the size of the matrix m. The numerical results given in this section attempt to answer this question for NC = 12, and for various values of INCMAX, i.e. blocks of the type illustrated in Tables 1 and 2. The parameters employed are $\alpha = 10\,\text{THz}$, $\beta = 0.1\,\text{THz}$; $\gamma = 5\,\text{THz}$, for a potential of the type $V = -V_0 \cos 2\theta(t)$. (For 40 blocks the matrix size is 1000 x 1000.)

For INCMAX = 4 (4 blocks) three major peaks appear in the far infra-red spectrum from eqn. (8), or equivalently, eqn. (6). These are illustrated in Fig.2(a). There is a further very small peak at $206\,\text{cm}^{-1}$. The matrix size is now 100 x 100. With INCMAX = 8 (200 x 100 matrix), there are five peaks visible in Fig. 2(b), whose positions and relative intensities have changed relative to Fig. 2(a). In Fig. 2(c), INCMAX = 16 (400 x 400 matrix), and five major peaks are visible. The two peaks at $118\,\text{cm}^{-1}$ and $180\,\text{cm}^{-1}$ stay roughly in the same position, those at $10\,\text{cm}^{-1}$ and $51\,\text{cm}^{-1}$ shift slightly to higher frequency. The obvious difference between Fig. 2(b) and Fig. 2(c) is the greatly diminished height of the peak at $146\,\text{cm}^{-1}$ ($m \equiv 200 \times 200$).

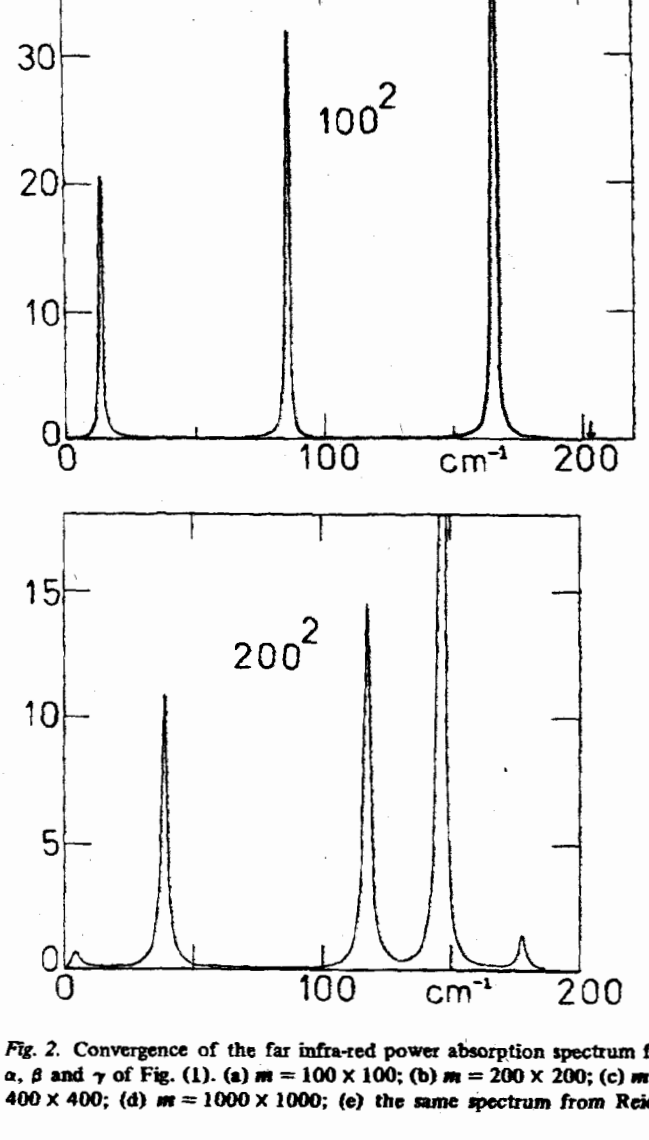

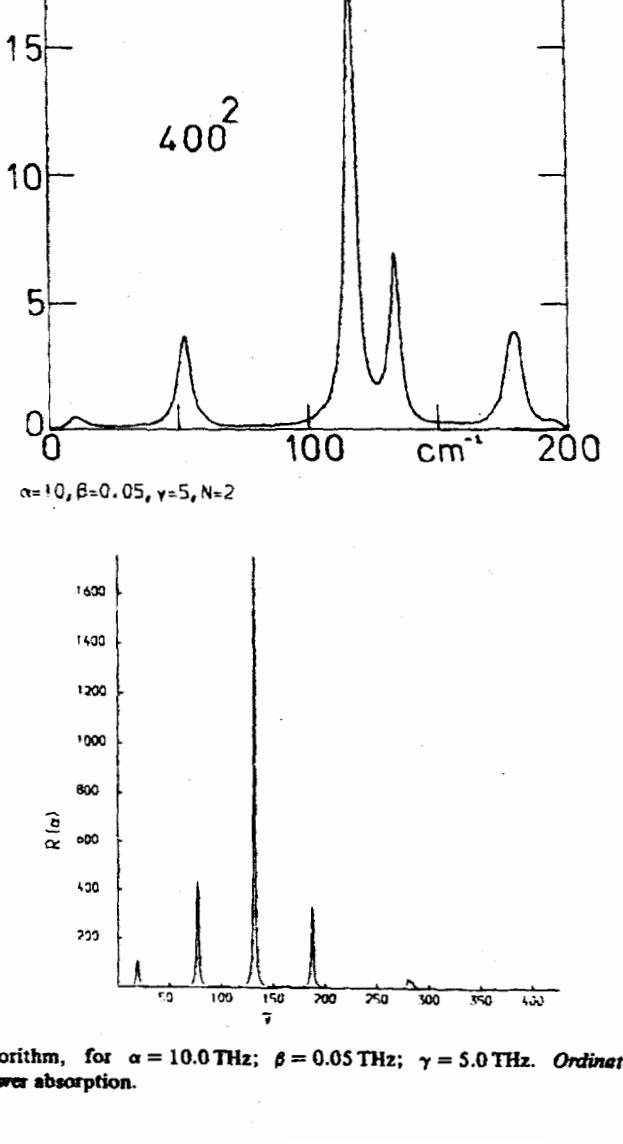

Fig. 2. Convergence of the far infra-red power absorption spectrum for α, β and γ of Fig. (1). (a) $m = 100 \times 100$; (b) $m = 200 \times 200$; (c) $m = 400 \times 400$; (d) $m = 1000 \times 1000$; (e) the same spectrum from Reid's algorithm, for $\alpha = 10.0\,\text{THz}$; $\beta = 0.05\,\text{THz}$; $\gamma = 5.0\,\text{THz}$. *Ordinate*: power absorption.

This has shifted towards the 118 cm^{-1} peak, which has increased in intensity a little and has stayed at the same frequency. The matrix m now contains *one hundred times* more elements than used in the production of Fig. 2(a), and it is possible to invert it only on a fast vector processor such as the CDC Cyber 205. (The memory limit of the CDC 7600 is exceeded at $m \equiv 200 \times 200$, being then some 7 times slower than the Cyber 205).

The results from Fig. 2(c) can be compared with those from Reid's algorithm for the same parameters α, β and γ (Fig. 2(d)). The Reid algorithm is structured wholly differently, but is written [2] for potentials of the type $V = -V_0 \cos 2m\theta(t)$ only. By making use of symmetry Reid has reduced the size of the matrix needed to obtain the far infra-red spectrum. His equivalent of matrix m need not be square, and for a rectangular Reid matrix containing the equivalent of 300 r terms and 6 blocks of the type described in his paper we obtain Fig. 2(d).

Experimental results and discussion

Kramers equations of the type (6) are now known [5] to be applicable in many fields of physics, astronomy and population genetics. The $\beta \to 0$ behaviour of such equations can, for example, be used [6] to describe the recently discovered [7] phenomenon of resonance activation of Josephson junctions by microwave irradiation. The peaks illustrated in Fig. (2) correspond [8] to specific phase angle fluctuation phenomena when the dissipation rate becomes very low, *even in the complete absence of irradiation*.

In the field of molecular dynamics, G. J. Evans [9] has recently reported the appearance of peaks in the far infra-red power absorption of a range of molecular liquids. The appearance of these peaks in liquid water has also been reported by Stanevich et al. [10], and has been corroborated by G. J. Evans and Nicolet Instruments Ltd. with an independent interferometric method [11]. The three independent observations of the water peaks are summarized in Table 3. Stanevich et al. [10] used a *grating* spectrometer, and G. J. Evans [11] used (i) an N.P.L./Grubb–Parsons *interferometer*; (ii) the independent Nicolet interferometer. It seems very unlikely, therefore, that these peaks are artifacts of the observational method. In the context of this paper it is also significant that liquid water is well known to be hydrogen-bonded [5], so that rates of escape from intermolecular potential wells are expected to be slowed by this binding of the molecules. As discussed already this implies that β is small, because the rate of escape from the Kramers equation in this limit becomes proportional [3, 5] to β.

Table III. *Liquid water: Far Infra-red peaks with different instruments* ($\bar{\nu}$) cm^{-1})

Stanevich and Yaroslavskii [10] (Grating Spectrometer)	G. J. Evans [9, 11] (Grubb/Parsons-Cube Interferometer)	G. J. Evans [11] (Nicolet Instruments Ltd. Interferometer)
160	162	161.0
–	165	167.0
173	175	173.5
191	188	191.0
–	197	198.0
210	210	210.0
–	out of	221.0
232	range	233.0

If we make a rough, order of magnitude, estimate of the parameter α for water, we have $I \doteq 2 \times 10^{-40}$ gm cm^2, so that at 300 K, $\alpha \doteq 15.0$ THz. A value of 0.1 THz for the parameter β means, very roughly speaking, an escape every 10 ps or so, i.e., a H-bond is broken and reformed, on the average, in this interval of time. This is a *simplistic* picture, but nevertheless acceptable as a rough description of what happens to an *individual* water molecule on the picosecond time-scale with which we are concerned. It is clear from Figs. (2) that α, β and γ of this order produce several far infra-red peaks, even for a potential $V = -V_0 \cos 2\theta(t)$ which is *known* to be far too simple for water. We have already mentioned how more realistic intermolecular potential can be obtained by Fourier synthesis, and how each term in the Fourier sum generates more peaks in the far infra-red spectrum. The Kramers equation is therefore fully capable of generating all the peaks listed in Table 3. It is probable that further observation will reveal yet more far infra-red peaks in liquid water. Matching these peaks to the appropriate Fourier series will provide information on the effective intermolecular potential and its spatial symmetry projected on to the plane of rotation (i.e. the "orbit" described by the angle θ). With computer simulation of Langevin dynamics, three dimensional analyses should be feasible.

In this context, the use of parameters equivalent to $\alpha = 15.0$ THz, $\beta = 0.1$ THz provides a new and simple explanation for the observed dielectric loss peak of liquid water, which occurs in the MHz–GHz range of frequencies. These parameters in eqn. (6) produce a *broad* dielectric loss curve (see Fig. (4)) precisely in this frequency range, *even though the moment of inertia used,* $I = 2 \times 10^{-40}$ *gm* cm^2, *is that of a single water molecule.* It is basically important to realize that eqn. (6) is therefore capable of reproducing two *apparently* quite different experimental aspects of liquid water molecular dynamics self-consistently and simply by using the limit $\beta \to 0$. In other words, eqn. (6) describes *both* the observed (Debye type) dielectric loss [5] *and* far infra-red peaks in the limit $\beta \to 0$.

Peaks have now been reported by G. J. Evans [9, 11] in several other dipolar and non-dipolar molecular liquids, including chlorobenzene, bromobenzene and benzene, where the positions of the lattice modes in the equivalent molecular crystals are well-known. These results await corroboration, but it is clear that the liquid state peaks occur closely in the vicinity of the crystal lattice modes. The agreement is particularly striking for chlorobenzene and benzene. There seem to be more peaks in the molecular liquid than in the corresponding crystal. This pattern is repeated for chloroform, deuterated chloroform, acetone, the (–) enantioner and racemic mixture of 2 chloro–butane, carbon tetrachloride, nitromethane, acetonitrile, and, of course, liquid water, where the liquid peaks (Table 3), are far more numerous than the lattice modes of ice at 1 bar just below the melting point [5]. These observations can be explained quite straightforwardly in terms of the symmetry of a sum such as eqn. (17). The greater the number of terms the lower the effective symmetry, and the more the number of far infra-red peaks. The effective symmetry in the liquid is known to be less than that in the crystalline solid, although recent diffraction studies [12] imply that the difference in local order is far smaller than expected. Similar conclusions come from the computer simulations of Rahman [13] on atomic liquids.

Some numerical results from Eqn. (6)

Figure (3) illustrates the development of peaks from Reid's

α=8, β=50, γ=10, N=2

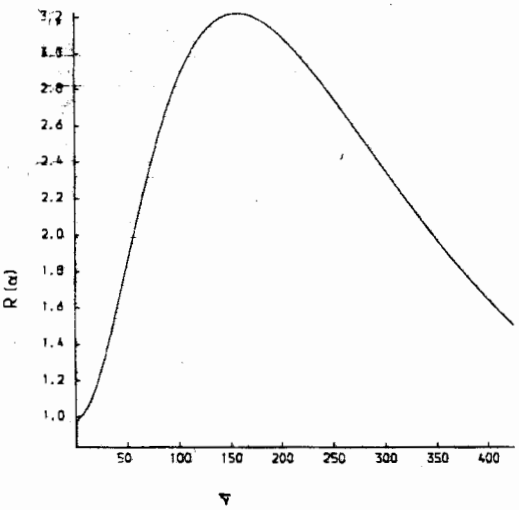

α=8, β=1.0, γ=10, N=2

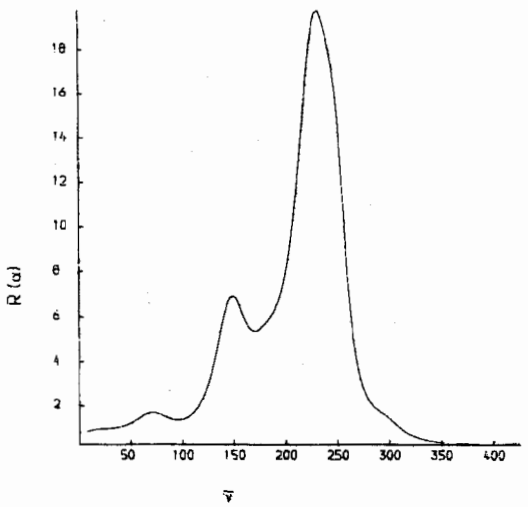

α=8, β=10, γ=10, N=2

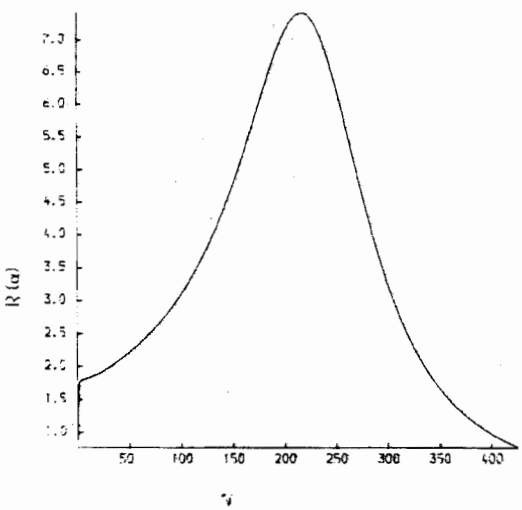

α=8, β=0.5, γ=10, N=2

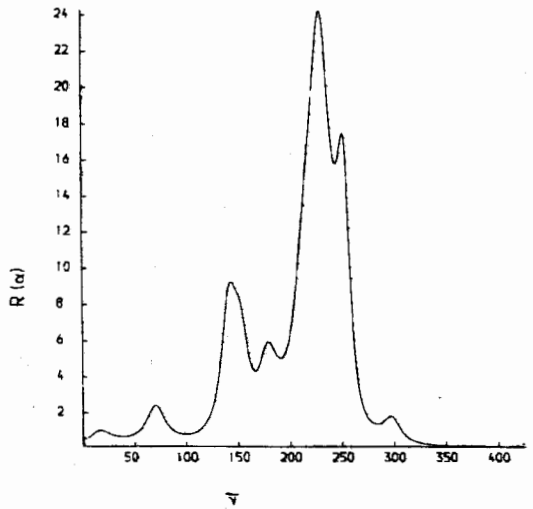

α=8, β=5, γ=10, N=2

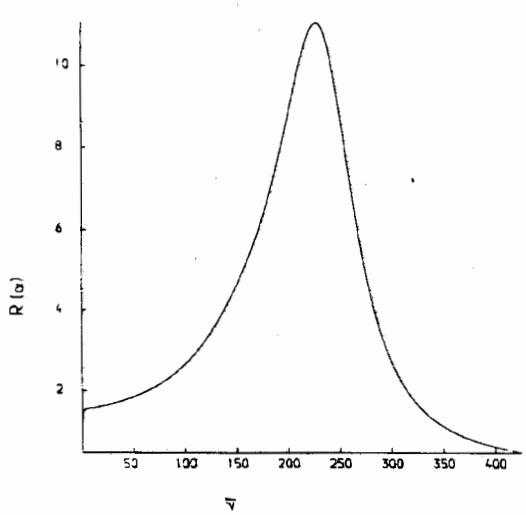

α=8, β=0.3, γ=10, N=2

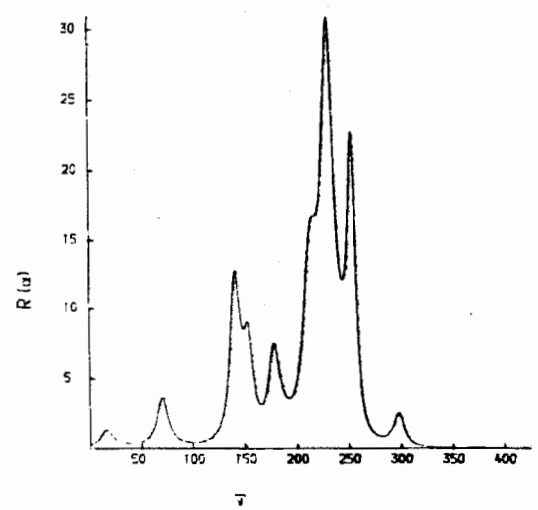

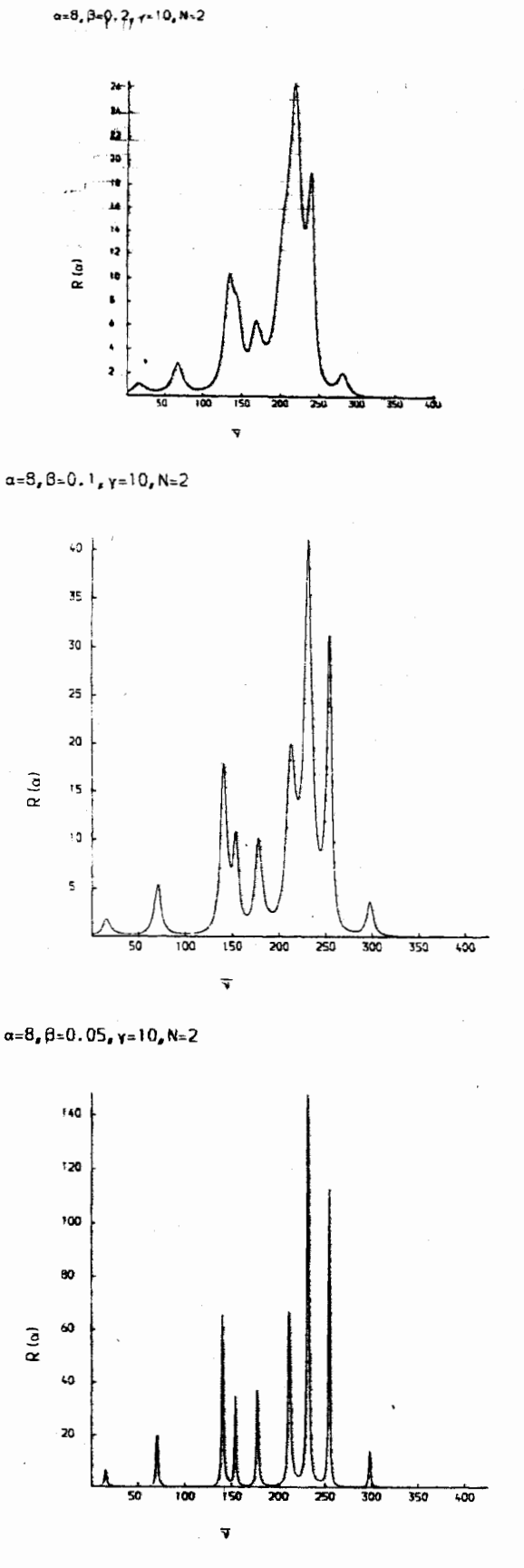

Fig. 3. Development of structure in the far infra-red power absorption from Reid's algorithm: $\alpha = 8.0$ THz; $\gamma = 10.0$ THz; (a) $\beta = 50.0$ THz; (b) $\beta = 10.0$ THz; (c) $\beta = 5.0$ THz; (d) $\beta = 1.0$ THz; (e) $\beta = 0.5$ THz; (f) $\beta = 0.03$ THz; (g) $\beta = 0.2$ THz; (h) $\beta = 0.1$ THz; (i) $\beta = 0.05$ THz. These spectra are computed with Reid's parameters[2]: $mm = 6$, $mp = 30$. *Ordinate*: power absorption.

algorithm [2] as $\beta \to 0$. The parameters are: $\alpha = 10.0$ THz, $\beta = 0.1$ THz and $\gamma = 8.0$ THz, and the potential $V = -V_0 \cos 2\theta(t)$. Some of the equivalent loss curves are illustrated in Fig. (4). Figures (4) show clearly that the *complete* loss profile from eqn. (6) is *a low frequency broad band together with a series of peaks in the far infra-red*. It is important in the light of Fig. (2) to estimate how many of these peaks are likely to be present for an effectively infinite matrix $\boldsymbol{m}$, when convergence has been attained. In this context it is known [2] that convergence is more rapid the larger the parameter β. It seems safe to assume therefore that the peaks, when first resolved in Fig. 3(d), for $\beta = 1.0$ THz, have come from a converged solution. Again, for a potential $V = -V_0 \cos 2\theta(t)$, there are five visible peaks in Fig. 3(d) as for the larger matrices in Fig. (2). As β is lowered from 1.0 to 0.5 THz further peaks are resolved (Fig. 3(e)), but thereafter the number does *not* increase. Nine peaks *only* remain at $\beta = 0.05$ THz (Fig. 3(i)), at exactly the same frequencies as with $\beta = 0.5$ THz. *For a given matrix size*, therefore, there is no dependence on β of the number of peaks in the spectrum.

The dependence of the number of peaks on the size of $\boldsymbol{m}$ is illustrated in Fig. (2) and has also been investigated recently by P. Grigolini and co-workers [14], who came to the important conclusion that in the low friction limit *the deterministic character of the system becomes dominant*. For a potential of the type $V = -V_0 \cos \theta(t)$ at low temperature, so that only the first two terms in the McLaurin expansion of $\cos \theta(t)$ are retained the so-called Duffing oscillator, two peaks appear for an effectively infinite matrix $\boldsymbol{m}$. These are also described by Voigtlaender and Risken [15], who claim that their numerical results agree with the deterministic limit $\beta \to 0$ calculated using an independent analytical method. The same two peak frequencies are observed by Grifolini and co-workers [14] using a continued fraction method, but the use of analogue circuit simulation [5] suggests the presence of a residual linewidth, and *importantly, a phase transition to deterministic chaos* as $\beta \to 0$. Voigtlaender and Risken [15], on the other hand, argue that the peaks survive unmasked by deterministic chaos even for β as low as 0.01 for precisely the same system as described by Grigolini et al. [14].

The question of how many peaks survive for an infinite matrix $\boldsymbol{m}$ is therefore a matter for further investigation and is of great interest. In our opinion the peaks in Figs. (2–4) are real, although some may diminish in intensity (see Fig. (2)) or shift in frequency as $\boldsymbol{m}$ is increased. One of the many interesting consequences of this work is that seemingly deterministic equations such as (17) show the phenomenon of so-called "transition to chaos", i.e. the trajectories defined by such equations become *exceedingly* complicated [16]. "Coupled pendulum" equations are well-known to show deterministic transition to chaos, a type of phase transition.

To end this discussion we look at two simple linear models, and provide a simple proof that more than one peak must exist in the far infra-red as the friction coefficient β vanishes. This proof is independent of the considerations by Grigolini et al. [14] and by Voigtlaender and Risken [15].

The harmonic oscillator [1, 2]

This is eqn. (6) in the limit $\sin \theta(t) \doteq \theta(t)$, i.e.:

$$I\ddot{\theta}(t) + I\beta\dot{\theta}(t) + m^2 V_0 \theta = \dot{w}(t) \qquad (24)$$

i.e. Hooke's law perturbed with friction and noise. If we write:

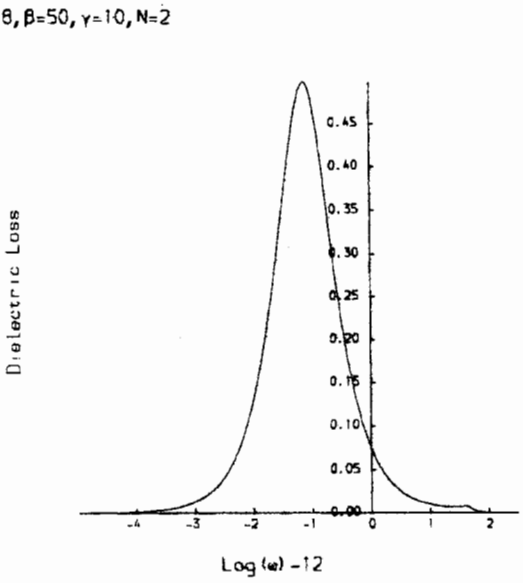

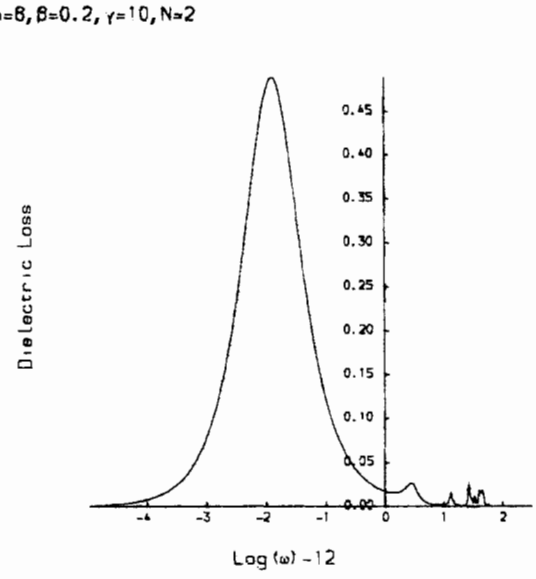

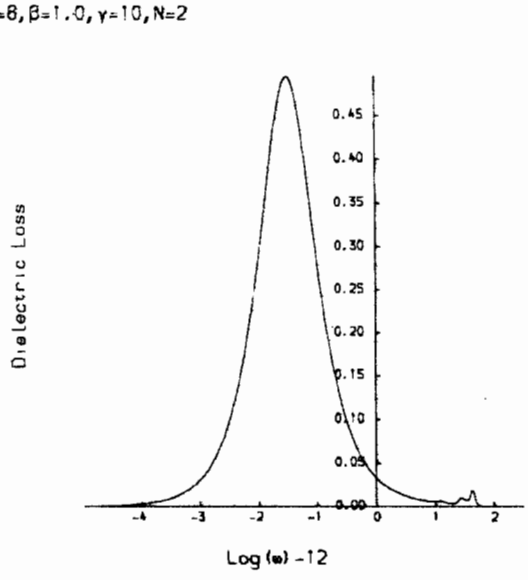

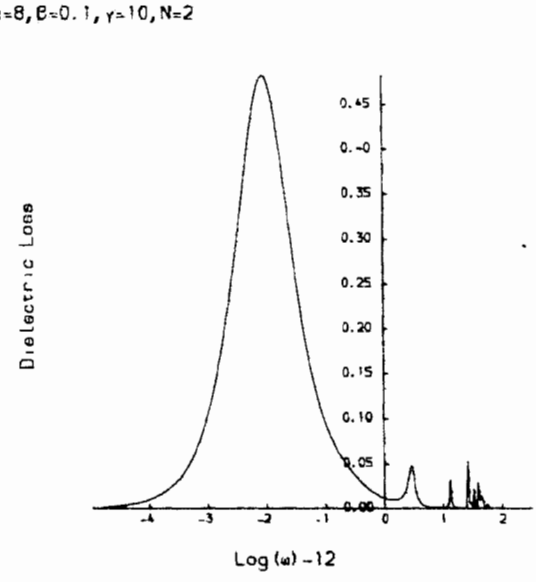

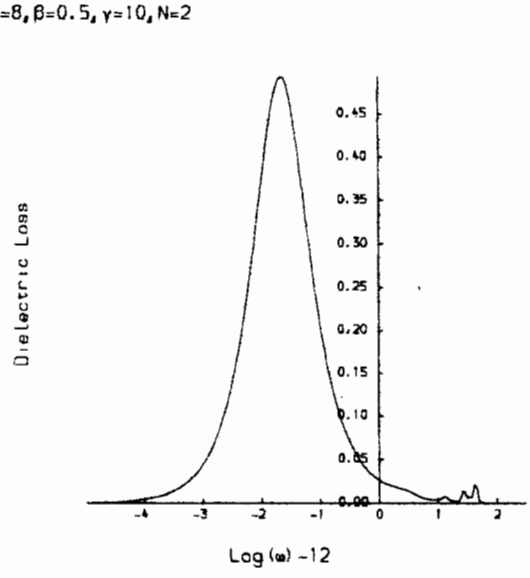

Fig. 4. **As for Fig. (3), dielectric loss $\alpha = 8.0$ THz, $\gamma = 10.0$ THz; (a) $\beta = 50.0$ THz; (b) $\beta = 1.0$ THz; (c) $\beta = 0.5$ THz; (d) $\beta = 0.2$ THz; (e) $\beta = 0.1$ THz. Note that the complete dielectric loss spectrum is a broad band of constant half-width at low frequencies, with a series of peaks developing on the high frequency side (in the far infra-red range). *Abscissa*: (log 10 (ω) − 12).**

$$\omega_0^2 \equiv \frac{m^2 V_0}{I} \tag{25}$$

eqn. (24) is well-known [2] to provide the following results:

$$\langle \dot{\theta}(t)\dot{\theta}(0)\rangle = e^{-\beta t}\left[\cos\left(\frac{\beta_1 t}{2}\right) + \frac{\beta}{\beta_1}\sin\left(\frac{\beta_1 t}{2}\right)\right] \tag{26}$$

for underdamped motion. Here:

$$\beta_1 \equiv 2\left(\omega_0^2 - \frac{\beta^2}{4}\right)^{1/2}. \tag{27}$$

In eqn. (26), the term on the l.h.s., $\langle \dot{\theta}(t)\dot{\theta}(0)\rangle$, is the equilibrium, *thermodynamically averaged*, angular velocity correlation function, whose Fourier transform is therefore a spectrum in the usual way. In the limit $\beta = 0$ eqn. (26) gives:

$$\frac{\langle \dot{\theta}(t)\dot{\theta}(0)\rangle}{\langle \dot{\theta}(0)\dot{\theta}(0)\rangle}_{\beta=0} = \cos\frac{\beta_1 t}{2}. \tag{28}$$

The angular velocity spectrum is therefore two *delta functions* (i.e. an infinitely sharp peak) at the frequencies $\pm\omega_0(\equiv\beta_1/2)$. In the limit $\beta \to 0$, on the other hand, it is more instructive to look directly at the analytical Fourier transform of eqn. (26) i.e., the *complete* spectrum. In this respect it is necessary to consider $0 \leqslant t \leqslant \infty$, so that the single-sided Fourier transform is defined as:

$$\mathscr{L}\langle \dot{\theta}(t)\dot{\theta}(0)\rangle = \int_0^\infty e^{-\beta|t|}e^{-i\omega t}\left(\cos\frac{\beta_1 t}{2} + \frac{\beta}{\beta_1}\sin\frac{\beta_1 t}{2}\right)dt$$

$$= \frac{1}{2}\left[\left(\frac{\beta}{\beta^2 + \left(\omega + \frac{\beta_1}{2}\right)^2} + \frac{\beta}{\beta^2 + \left(\omega - \frac{\beta_1}{2}\right)^2}\right)\right.$$

$$\left. + i\left[\frac{\left(\frac{\beta_1}{2} - \beta\right)}{\beta^2 + \left(\frac{\beta_1}{2} - \omega\right)^2} - \frac{\left(\frac{\beta_1}{2} + \beta\right)}{\beta^2 + \left(\frac{\beta_1}{2} + \omega\right)^2}\right]\right]$$

$$+ \frac{\beta}{2\beta_1}\left[\left(\frac{(\beta_1/2 - \beta)}{\beta^2 + (\beta_1/2 - \omega)^2} + \frac{\beta_1/2 + \beta}{\beta^2 + (\beta_1/2 + \beta)^2}\right)\right.$$

$$\left. + i\left(\frac{\beta}{\beta^2 + \left(\frac{\beta_1}{2} + \omega\right)^2} - \frac{\beta}{\beta^2 + \left(\frac{\beta_1}{2} - \omega\right)^2}\right)\right] \tag{29}$$

The *complete* analytical spectrum from eqn. (24) therefore consists of several peaks. In the range of physical interest, i.e. $0 \leqslant \omega \leqslant \infty$, there are three peaks in the real part of eqn. (29). One of these is situated at $\omega_1 = \beta_1/2$, and is a positive peak of approximate height $+ 1/2\beta$ and half width β. As $\beta \to 0$ this therefore becomes the delta function mentioned already. However, there are two more peaks for finite β whose intensities are proportional to β/β_1 for all $\omega \geqslant 0$. These disappear if and only if β *vanishes* (i.e. $\beta \equiv 0$). The approximate heights of these peaks are $\pm 1/4\beta$, with half width β; and they are situated at $(\beta_1/2 \pm \beta)$. In the simple linear case of eqn. (24) the three peaks in the limit $\beta \to 0$ therefore *happen to be situated at the same frequency*. In the non-linear case this might well no longer be so.

The linear itinerant oscillator

This is well-known to be the next approximant [5] of the same linear Mori continued fraction [17] which generates the harmonic oscillator. The angular velocity a.c.f. in this case can be written as:

$$\frac{\langle \dot{\theta}(t)\dot{\theta}(0)\rangle}{\langle \theta(0)\theta(0)\rangle} = \frac{e^{-\sigma_1 t}\cos\omega_1 t}{1+\Lambda} + \left(\frac{\sigma_1}{\omega_1}\right)\frac{e^{-\sigma_1 t}\sin\omega_1 t}{1+\Lambda}$$

$$+ \left(\frac{\sigma_2}{\omega_1}\right)\frac{\Lambda e^{-\sigma_1 t}\sin\omega_1 t}{1+\Lambda} + \frac{\Lambda}{1+\Lambda}e^{-\sigma_2 t} \tag{30}$$

The complete Fourier transform of eqn. (30) therefore consists, on the positive frequency side, of several peaks defined as follows.

(i) A Lorentzian centred at the frequency origin ($\omega = 0$) of height $\Lambda(1+\Lambda)^{-1}\sigma_2^{-1}$ and half-width σ_2.

(ii) A Lorentzian centred at $\pm\omega_1$ of height $+\frac{1}{2}(1+\Lambda)^{-1}\sigma_1^{-1}$ and half-width σ_1.

(iii) Positive and negative peaks at $\omega_1 \mp \sigma_1$ respectively, of approximate height (or depth)

$$\left(\frac{\sigma_1}{\omega_1}\right)\cdot\frac{1}{4\sigma_1(1+\Lambda)}.$$

(iv) Positive and negative peaks at $\omega_1 \mp \sigma_1$ respectively, of approximate height (or depth)

$$\left(\frac{\sigma_2}{\omega_1}\right)\cdot\frac{\Lambda}{4\sigma_1(1+\Lambda)}.$$

The low friction limit of the linear itinerant oscillator, eqn. (30), means that *both* σ_1 and σ_2 tend to zero. When $\sigma_1 = \sigma_2 = 0$ we recover the deterministic spectrum, which consists of two delta functions, one at the origin ($\omega = 0$) and one at $\omega = \omega_1$. (In this respect note that the deterministic angular velocity spectrum from the zeroth linear Mori approximant, eqn. (1), is a single delta function at $\omega = 0$.)

In summary, therefore, the deterministic spectra from the linear Mori continued fraction consist of delta functions. For approximant zero [eqn. (1)] there is one delta function at the origin. For approximant one [eqn. (24)] there is one delta function at $\omega = \beta_1/2$. For approximant two (eqn. (30)] there are two delta functions: one at $\omega = 0$ and one at $\omega = \omega_1$. In general it is known that the angular velocity correlation function from the linear Mori continued fraction is an infinite sum of complex exponentials. This leads to the conclusion that the deterministic angular velocity spectrum from high order *linear* Mori approximants [18] will consist of a large number of delta functions (see appendix). Therefore, *in the linear case*, peaks are expected in the far infra-red power absorption in the low friction limit.

Grigolini et al. [14] have, however, just made the important discovery that when the analysis is extended to the *non*-linear case, the *deterministic* trajectories *themselves* become so intricately complicated [16] that *some*, but *not all* of these delta functions may be masked by a residual uncertainty (i.e. linewidth) and, at a well-defined value of the friction coefficient, are suddenly *shifted in frequency* because of the sudden onset of "deterministic chaos". Grigolini et al. [14] have therefore discovered a *fundamentally* new phenomenon of *deterministic physics in the low friction limit*.

Acknowledgements

The University of Wales and S.E.R.C. are thanked for financial help. This work benefitted greatly from discussions with Prof. P. Grigolini and co-workers at Pisa.

References

1. Evans, M. W., Evans, G. J., Coffey, W. T. and Grigolini, P., Molecular Dynamics, chapter 2, Wiley/Interscience, N.Y., (1982).
2. Reid, C. J., Mol. Phys., 49, 331 (1983).
3. Risken, H., "The Fokker–Planck Equation", Springer Series in Synergetics, Vol. 18 Springer, Berlin (1984).
4. Landau, L. D. and Lifshitz, E. M., "Statistical Physics", p. 207 ff (e.g. their eqn. (69.4)), 3rd edition, Pergamon, Oxford (1980).
5. For a series of reviews see vols. 62 and 63 of "Advances in Chemical Physics", Edited by Evans, M. W., Grigolini, P. and Pastori-Parravicini, G., gen. Edited by Prigogine and Rice, Wiley/Interscience, N.Y. (1985), in press.
6. Fonseca, T. and Grigolini, P., Phys. Rev. A., submitted, preprint kindly sent to one of us (MWE) by Grigolini, P. (March, 1985).
7. Devoret, M. H., Martinis, J. M., Esteve, D. and Clarke, J., Phys. Rev. Lett., 53, 1260 (1984).
8. Evans, M. W., Phys. Lett., A106, 155 (1984).
9. Evans, G. J., J. Chem. Soc., Faraday Trans. 11, 79, 547 (1983); in press, (1985).
10. Stanevich, A. E. and Yaroslavskii, N. G., Opt. Spectrosc., 11, 276 (1961).
11. Evans, G. J., unpublished, data kindly sent in unpublished form to MWE, August (1984).
12. Bisanti, P. and Sacchetti, F., Mol. Phys., 54, 255 (1985).
13. Rahman, A., Phys. Rev. Lett., 32, 52 (1973).
14. Fronzoni, L., Grigolini, P., Mannella, R. and Zambon, B., preprint kindly sent to MWE (March, 1985).
15. Voigtlaender, K. and Risken, H., J. Stat. Phys., submitted (preprint kindly sent to MWE), (April, 1985).
16. Huberman, B. A., and Crutchfield, J. P., Phys. Rev. Lett., 43, 1743 (1979); Bohr, T., Bak, P. and Jensen, M. H., Phys. Rev., 30A, 1970 (1984).
17. ref [1], chapters 1–4.
18. Evans, M. W., Chem. Phys. Letters, 48, 385 (1977).

Appendix

It has been shown [18] that the angular velocity a.c.f. from the third linear Mori approximant takes on three general forms, i.e.:

$$C(t) = {}^0x_0\, e^{-\alpha_1 t}\cos\beta_1 t + {}^0x_1\, e^{-\alpha_1 t}\sin\beta_1 t + {}^0x_2\, e^{-\alpha_2 t}\cos\beta_2 t + {}^0x_3\, e^{-\alpha_2 t}\sin\beta_2 t \qquad \text{(A1)}$$

where the x coefficients can be described in terms of the roots: $(\alpha_1 + i\beta_1), (\alpha_1 - i\beta_1), (\alpha_2 + i\beta_2)$, and $(\alpha_2 - i\beta_2)$; or:

$$C(t) = {}^1x_1\, e^{-\alpha_1 t} + {}^1x_2\, e^{-\alpha_2 t} + {}^1x_3\, e^{-\alpha_3 t}\cos\beta_3 t + {}^1x_4\, e^{-\alpha_4 t}\sin\beta_3 t \qquad \text{(A2)}$$

or

$$C(t) = \sum_n^4 D_n \exp(-\alpha_n t). \qquad \text{(A3)}$$

In the deterministic limit eqn. (A1) provides *two distinct peaks*; *two* delta functions at $\omega = \beta_1$ and $\omega = \beta_2$. Eqn. (A2) provides *three peaks*; two delta functions superimposed at the origin, $(\omega = 0)$, and another at $\omega = \omega_3$. Eqn. (A3) provides *four delta functions*, superimposed at $\omega = 0$.

This argument can be *extended to higher* approximants.